



POLITECNICO
MILANO 1863

RE.PUBLIC@POLIMI

Research Publications at Politecnico di Milano

Post-Print

This is the accepted version of:

M. Hernández, M. Mar Bernal, A.M. Grande, N. Zhong, S. van der Zwaag, S.J. García
Effect of Graphene Content on the Restoration of Mechanical, Electrical and Thermal Functionalities of a Self-Healing Natural Rubber
Smart Materials and Structures, Vol. 26, N. 8, 2017, 085010 (10 pages)
doi:10.1088/1361-665X/aa71f5

The final publication is available at <https://doi.org/10.1088/1361-665X/aa71f5>

Access to the published version may require subscription.

When citing this work, cite the original published paper.

Permanent link to this version

<http://hdl.handle.net/11311/1031684>

Effect of Graphene Content on the Restoration of Mechanical, Electrical and Thermal Properties of a Self-Healing Natural Rubber

Marianella Hernández^{1,*}, M. Mar Bernal², Antonio M. Grande¹, Nan Zhong¹, Sybrand van der Zwaag¹ and Santiago J. García^{1,*}

¹*Novel Aerospace Materials Group, Faculty of Aerospace Engineering, Delft University of Technology, Kluyverweg 1, 2629 HS Delft, the Netherlands*

²*Institute of Polymer Science and Technology (ICTP-CSIC), Juan de la Cierva 3, Madrid 28006, Spain*

*corresponding authors: m.hernandezsantana-1@tudelft.nl / s.j.garciaespallargas@tudelft.nl.
Telephone number: +31(0)15 2781637

Abstract

In this work we show the effect of graphene loading on the restoration of the mechanical properties and thermal and electrical conductivity of a self-healing natural rubber nanocomposite. The graphene loading led to a minimal enhancement of mechanical properties and yielded a modest increase in thermal and electrical conduction. The polymer nanocomposites were macroscopically damaged (cut) and thermally healed for 7 hours in a healing cell. Different healing trends as function of the graphene content were found for each of the functionalities: (i) thermal conductivity was fully restored independently of the graphene filler loading; (ii) electrical conductivity was restored to a high degree only above the percolation threshold; and (iii) tensile strength restoration increased more or less linearly with graphene content but was never complete. A molecular dynamics analysis by dielectric spectroscopy of the pristine and healed samples highlighted the role of graphene-polymer interactions at the healed interphase on the overall restoration of the different functionalities. Based on these results it is suggested that the dependence of the various healing efficiencies with graphene content is due to a combination of the graphene induced lower crosslinking density, as well as the presence of strong polymer-filler interactions at the healed interphase.

Keywords: Nanocomposites; Rubber; Self-healing; Mechanical properties; Electrical properties

1. Introduction

Graphene has attracted significant attention in the field of polymer nanocomposites for its possibility to develop multifunctional polymers with electrical, thermal, barrier and increased

mechanical properties.[1,2] The properties of graphene nanocomposites based on rubber matrices has been addressed in a number of earlier publications. In particular, graphene filled natural rubber (NR) composites have caught major attention in the last decade due to their significant technological potential.[3-9] Yet, even improved materials are still prone to damage. A particularly attractive route to make such composites more durable is the use of self-healing concepts, *i.e.* materials capable of repairing damage rather than preventing it.[10,11] Several concepts have already been reported following this route. Xiao *et al*[12] reported epoxy-based shape memory composites with graphene contents of 0.0025 to 0.0125 vol% capable of undergoing thermally induced healing. In a different approach, Wang *et al*[13] described an elastic nanocomposite material with self-healing ability by combining the unique features of hydrogen-bonded polymers and graphene oxide (GO) as a macro-crosslinker. By adding as little as <2 wt% of GO to the supramolecular polymer, they obtained an elastic material with similar mechanical properties to that of conventional rubbers while possessing very fast healing properties at room temperature. Huang *et al*[14] also reported excellent healing efficiencies in thermoplastic polyurethane/graphene composites using three different external stimuli (*e.g.* IR light, electricity and electromagnetic wave). While Liu *et al*[15] described the self-healing capability of graphene nanocomposite hydrogels fabricated by using graphene peroxide as poly-functional initiating and crosslinking centers. Nevertheless, to the best knowledge of the authors no studies have previously been reported on graphene loaded self-healing NR nanocomposites.

In two of our previous works we reported on the development of a self-healing NR vulcanized using conventional sulfur curing systems.[16,17] In the present work we introduce a multifunctional self-healing NR/graphene nanocomposite and study the effect of graphene loading on the restoration of mechanical, thermal and electrical properties. Several studies have recently been reported focusing on the restoration of only one functional property in filled self-healing matrices,[18,19] but this paper could be a first in reporting both mechanical and healing efficiencies of two functional properties. The role of the nanocomposites molecular dynamics (and the way it is affected by the presence of graphene) in the restoration of all functionalities (mechanical and conductive) is also underlined.

2. Experimental

2.1. Materials and compounding

Natural rubber (NR) consisting of *cis*-1,4-polyisoprene chains was kindly supplied by *Malaysian Rubber* under the trade name SMRCV50 [Mooney viscosity, ML(1+4)100 °C=50].

The ingredients employed as vulcanizing additives in the preparation of NR compounds were all commercial grades and used as received. Graphene (avanGRAPHENE-2) supplied by *Avanzare* was used as nanofiller in different amounts (0, 0.25, 0.50, 1.0 and 2.0 phr). Rubber compounds were prepared according to the recipe shown in Table 1 expressed in parts per hundred parts of rubber (phr) in weight. The selected compound recipe gives an optimal balance between healing and mechanical properties, as recently reported.[17]

Table 1. NR compound recipe.

Ingredient	Composition (phr)
NR	100
Zinc oxide (ZnO)	5
Stearic acid (SA)	1
N-cyclohexylbenzothiazole-2-sulphenamide (CBS)	0.26
Sulfur (S)	1.3
Graphene	0-2

Mixing was performed in an open two-roll mill (*Comerio Ercole MGN-300S*) at room temperature. The rotors operated at a speed ratio of 1:1.2. First, mastication of the rubber took place. The vulcanizing additives except sulfur were then added to the rubber prior to the incorporation of the filler and, finally, sulfur was added. Rubber compounds were vulcanized in an electrically heated hydraulic press (*Gumix*) at 150 °C and 200 MPa according to the optimum cure time (t_{90}) derived from the curing curves obtained from the rubber process analyzer (*Alpha Technologies RPA2000*) at T=150 °C, frequency 0.833 Hz and 2.79% strain. Specimens were mechanically cut out from the vulcanized rubber sheets. The average mass of network chains between crosslinks (crosslinking density, ν) was determined on the basis of solvent-swelling measurements in toluene by application of the Flory–Rehner[20] equation and assuming the formation of tetra-functional crosslinks during the vulcanization reaction.

2.2. Materials characterization

Nanocomposites morphology was investigated using a scanning electron microscope (SEM) *Jeol JSM-7500F*. The samples were freeze fractured below their glass transition

temperature ($T_g \sim -60$ °C) by cooling in liquid nitrogen. SEM images were obtained at 5 kV. *PerkinElmer* Fourier transform infrared (FT-IR) spectrometer was used in the wavenumber range of 1200-3200 cm^{-1} . All the spectra were baseline corrected and normalized using *PerkinElmer Spectrum* software.

Rectangular samples (70x10x2) mm were used for uniaxial tensile testing. Tests were done on a universal mechanical testing machine (*Instron 3365*) equipped with a 1 kN load cell. Samples were stretched until failure at a constant cross-head speed of 1 mm/s at room temperature. Ultimate stress, ultimate strain and instantaneous modulus were determined in order to mechanically characterize the NR composites and to evaluate their healing efficiency. Data reported represent the average value from at least three samples.

Broadband dielectric spectroscopy (BDS) measurements were performed on an ALPHA high resolution dielectric analyzer (*Novocontrol Technologies GmbH*). All samples (pristine and healed) were mounted in the dielectric cell between two parallel gold-plated electrodes. The complex permittivity $\varepsilon^*(\omega) = \varepsilon'(\omega) - i\varepsilon''(\omega)$ of each circular sample (20 mm diameter) was measured by performing consecutive isothermal frequency sweeps over a frequency window of $10^{-1} < f(\text{Hz}) < 10^7$ (where f is the frequency of the applied electric field) in the temperature range from -100 to 100 °C in steps of 5 °C. The AC conductivity was measured in the same conditions as $\varepsilon^*(\omega)$ and the results were given directly by the dielectric analyzer. In a conducting composite, the conductivity is composed of two terms:

$$\sigma(f) = \sigma_{dc} + Af^x \quad (1)$$

where σ_{dc} is the direct current conductivity, A is a constant and x is an exponent which describes the frequency (f) dependence of $\sigma(f)$. The term σ_{dc} appears as a plateau at low frequencies in the experiments and its value is obtained at 10^{-1} Hz.

1 mm thick circular samples (20 mm diameter) were used for measuring thermal conductivity. Samples were placed in contact with a single sided smooth aluminium foil before doing the tests. Measurements were done at room temperature using a modified transient source technique on a *TCi C-Therm* apparatus. Distilled water was used as the contact agent.

2.3. Healing procedure

Mechanical healing. Macroscopic damage was introduced to vulcanized rectangular samples by manually making a straight cut along the width using a fresh scalpel blade. The rectangular

damaged samples were carefully positioned inside a home-built healing cell between two glass plates such that the cut surfaces were in seemingly optimal initial contact (see [17] for further experimental details). The cut samples were subsequently healed under a controlled temperature ($T=70\text{ }^{\circ}\text{C}$) for 7 h while a constant pressure ($P=1\text{ bar}$) was applied to the confining plates. The application of pressure on the glass plates and the resulting lateral expansion of sample assures the presence of a controlled light contact pressure across the cut interface during healing. The healed samples were tested according to the tensile protocol described above.

Electrical and thermal conductivity restoration. Damage was introduced by making several cuts in various directions in the center of a 20 mm diameter circular vulcanized sample. The damaged sample was then placed in the healing cell at $70\text{ }^{\circ}\text{C}$ for 7 h for healing to take place. The electrical conductivity of the thermally healed system was measured again following the same conditions as for the pristine samples. To monitor the recovery of the thermal conductivity, damaged samples were prepared by doing superficial cuts using a razor blade in the whole surface area of the sample and bringing the rough surface in contact with the smooth aluminum foil. The damaged sample was then placed in the healing cell at $70\text{ }^{\circ}\text{C}$ for 7 h leading to a so-called healed sample. The thermal conductivity of the healed samples was measured accordingly.

The healing efficiency for each selected property was calculated as the ratio between the values under healed and pristine conditions according to:

$$\eta_p [\%] = \frac{P_{healed}}{P_{pristine}} \times 100 \quad (2)$$

where p is the property of interest (mechanical strength, electrical conductivity and thermal conductivity).

3. Results and discussion

3.1. Chemical and mechanical characterization of NR/graphene nanocomposites

Table 2 shows the crosslinking density derived from swelling tests for the different composites. Crosslinking density increases with graphene contents until 0.5 phr. After this point an apparent reduction in the crosslinking density was detected with the graphene content increase. This result is somewhat unexpected since graphene layers with their high specific area have been reported to induce stronger interfacial interactions with the NR matrix and act

as additional sources of entanglements or physical crosslinking points in composites.[6] Nevertheless, at higher graphene content the rubber-filler interactions seem to be lower as expressed by the ratio Q_f/Q_g compiled in Table 2, where Q_f and Q_g denote the swelling ratio of the filled and the unfilled rubber, respectively. Such a ratio reflects the restriction to swelling of the rubber matrix in the neighborhood of filler particles, since diffusion of solvent is impaired. The higher the Q_f/Q_g values, the lower will be the extent of interaction between the filler and the matrix.[21] Moreover, the filler might affect the efficiency of the curing agents disturbing the crosslinked network. Wu *et al*[8] reported that when graphene loading is lower than 0.3 phr, the curing agents (S + CBS) diffuse freely and the vulcanization reaction proceeds smoothly. But with higher graphene content the curing agents can be isolated by the graphene nanosheets and need to go through tortuous paths to form polysulfide species and crosslinking points. Curing agents, especially the CBS molecules with severe steric hindrance are more difficult to diffuse in the immobilized rubber chains between graphene layers.[8,22]

Table 2. Swelling ratio and crosslinking density of pristine NR/graphene nanocomposites.

Compound	Crosslinking density	Swelling ratio
	$\nu \cdot 10^{-4}$ (mol/g)	Q_f/Q_g
NR	3.46±0.08	---
NR/0.25	3.64±0.05	1.66±0.01
NR/0.5	4.65±0.04	1.57±0.02
NR/1.0	2.43±0.01	1.97±0.01
NR/2.0	3.05±0.06	2.34±0.03

FT-IR measurements corroborate such trend (see Figure 1). Observing the characteristic peak at 1596 cm^{-1} ascribed to C=C stretching of *cis*-1,4-polyisoprene units, one can notice that the lower intensity and lower peak area correspond to 0.5 phr of graphene. This could indicate that at such loading, the extent of chemical interactions are prominent due to the existence of strong π - π interactions between the π electrons of graphene and C=C bonds of isoprene units.[5] The intensity of the peak at 1596 cm^{-1} also reduces when healing takes place, regardless of the amount of graphene. This result is consistent with the observations from dielectric spectroscopy that will be discussed later on.

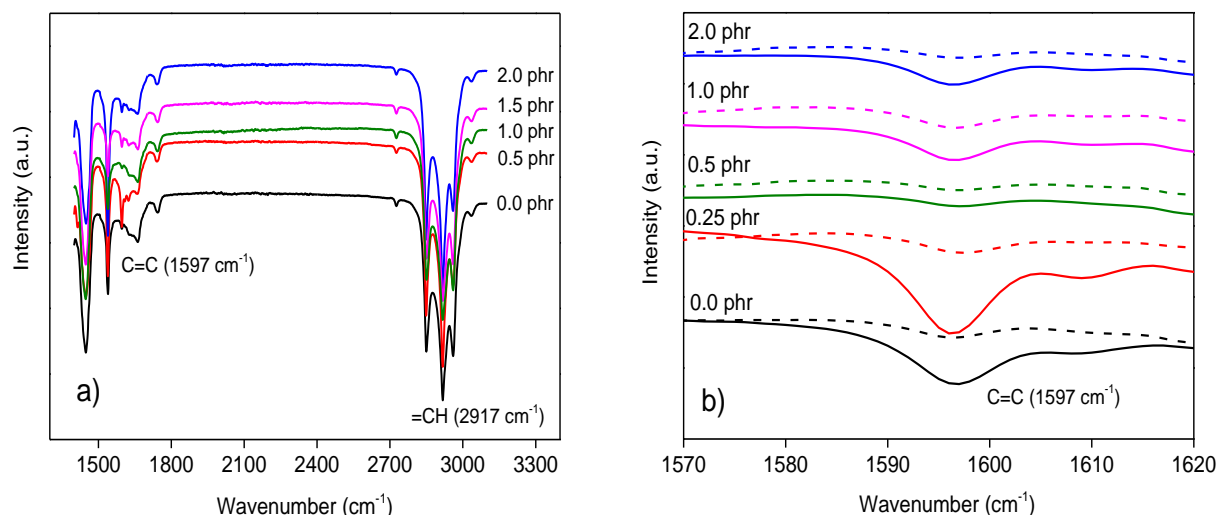


Figure 1. FT-IR spectra of NR/graphene nanocomposites: a) whole wavenumber range; b) at selected normalized region. Solid lines and dashed lines correspond to pristine and healed samples, respectively.

Table 3 summarizes mechanical properties data. The moderate reinforcement effect observed with graphene addition is in good agreement with the crosslinking density values shown above. Such low reinforcement may be due to problems with interfacial adhesion and spatial distribution of the filler, which typically govern the ultimate performance of polymer nanocomposites.[23] Moreover, the graphene layers have also been reported to disturb the “naturally occurring network” of NR producing dead ends and leading to lower mechanical properties at higher filler loadings.[24]

Table 3. Tensile properties of pristine and healed NR/graphene nanocomposites.

Compound	Instantaneous modulus (MPa)		Ultimate stress (MPa)		Ultimate strain (-)	
	pristine	healed	pristine	healed	pristine	healed
NR	0.25±0.03	0.16±0.02	0.48±0.02	0.21±0.04	4.23±0.17	0.86±0.10
NR/0.25	0.25±0.01	0.18±0.01	0.45±0.02	0.27±0.01	4.62±0.25	3.70±0.12
NR/0.5	0.27±0.02	0.20±0.02	0.56±0.04	0.30±0.02	5.69±0.43	2.38±0.37
NR/1.0	0.24±0.01	0.30±0.04	0.27±0.01	0.17±0.01	3.99±0.12	1.29±0.50
NR/2.0	0.22±0.01	0.17±0.01	0.35±0.01	0.24±0.03	4.59±0.08	3.14±0.30

A morphology study of the nanocomposites was performed to establish a clearer structure-property relationship. SEM images of the prepared nanocomposites are displayed in Figure 2. It is evident that graphene, seen as non-flat individual nanosheets, is uniformly distributed throughout the NR matrix at any concentration (see circled areas). However, at higher loading numerous graphene sheets are more clearly observed to pull out of the matrix giving an insight into the weak interfacial polymer-particle strength (see Figure 2d and e), thus affecting the mechanical performance of these nanocomposites.

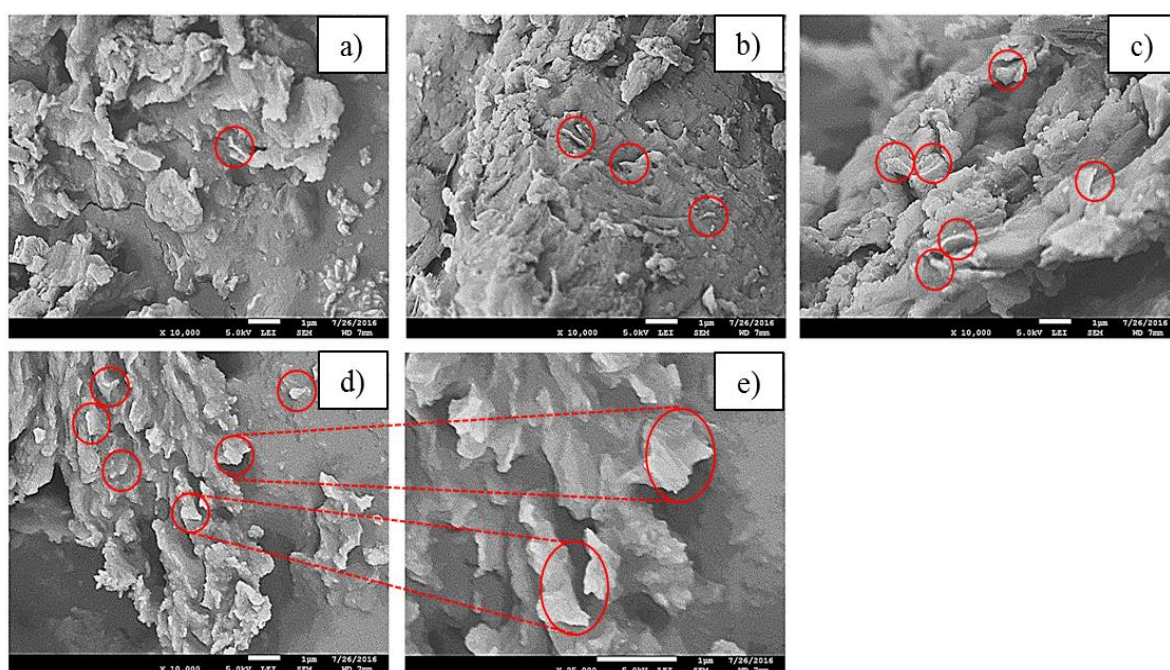


Figure 2. SEM images of pristine NR/graphene nanocomposites with different graphene loading: a) 0.25 phr; b) 0.5 phr; c) 1.0 phr; d) 2.0 phr; e) 2.0 phr at higher magnification.

3.2. Electrical and thermal conductivity of the NR/graphene nanocomposites

Figure 3a) illustrates the variation of electrical conductivity (σ) in the frequency domain with increasing nanofiller content at $T=70$ °C. At any given frequency, a modest conductivity increase with graphene loading can be seen. Although not shown here, at room temperature such an increase could not be detected due to limitations in the minimum frequency value set by the equipment. However, an increase in electrical conductivity with temperature is to be expected.[25] Numerous studies show that the percolation threshold and conductivity of nanocomposites depend strongly on the polymer matrix type, aspect ratio of filler, and uniform spatial distribution of individual filler, among others.[1,26,27] The good distribution

of graphene layers inside the NR matrix, as seen in Figure 2, and the possible interconnection between them can then explain the observed increase in conductivity. At the percolation threshold located between 0.25-0.50 phr graphene, the filler particles begin to contact each other, a conducting path is formed throughout the composite and a sudden increase in conductivity occurs (2 orders of magnitude), as seen in Figure 3b). The electrical properties of the nanocomposites, however, seem to be dominated by the non-conductive NR matrix, being the final conductivity values low, typically of semi-conducting materials. Other authors have reported similarly modest conductivity increments in rubber nanocomposites.[3,4,25]

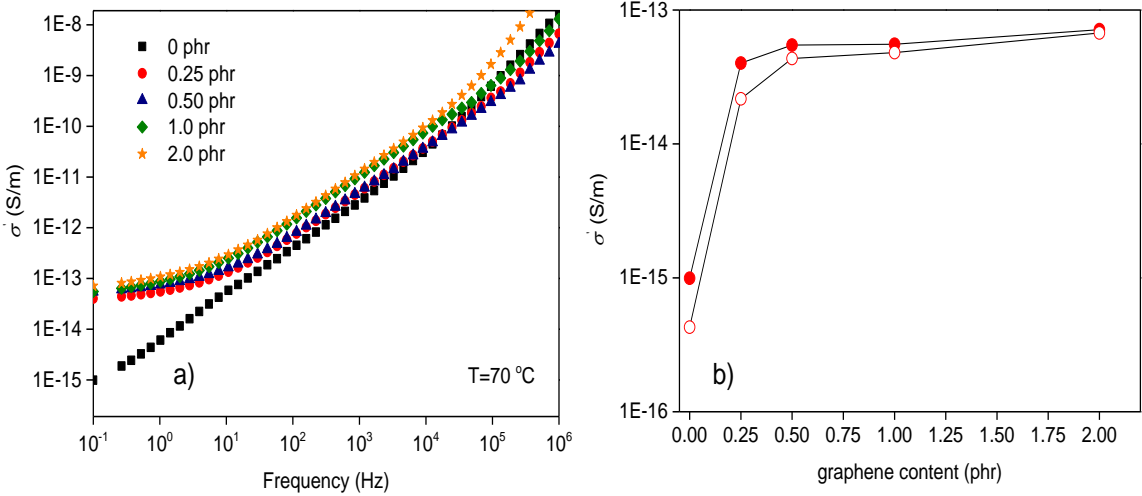


Figure 3. a) Electrical conductivity of pristine NR/graphene nanocomposites as function of frequency with graphene content as a parameter; b) Electrical conductivity of NR/graphene nanocomposites pristine and healed (at 70 °C), at a frequency of $f=10^{-1}$ Hz.

Many of the considerations discussed for mechanical reinforcement and electrical conductivity can also be applied for the thermal conductivity (κ). [1] Figure 4 shows the relative thermal conductivity with respect to the unfilled rubber as function of the graphene loading. A low increase ($\sim 5\%$) in thermal conductivity with graphene loading is observed. The volume dependence is rather weak. The thermal conductivity after damage and healing will be discussed in section 3.4.

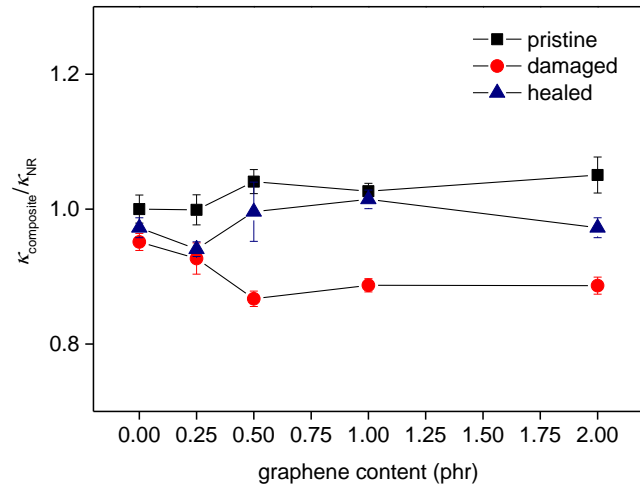


Figure 4. Relative thermal conductivity of pristine, damaged and healed NR/graphene nanocomposites as function of graphene content measured at room temperature.

3.3. Molecular dynamics of NR/graphene nanocomposites

Broadband dielectric spectroscopy (BDS) was used to investigate the effect of graphene content on the rubber molecular dynamics. Two relaxations were found on the dielectric spectra of the nanocomposites, as marked in Figure 5. From low to high temperatures, the segmental relaxation corresponding to the glass transition temperature (T_g) appears first at around -40 °C, and then at higher temperatures a second relaxation is detected only in the healed nanocomposites.

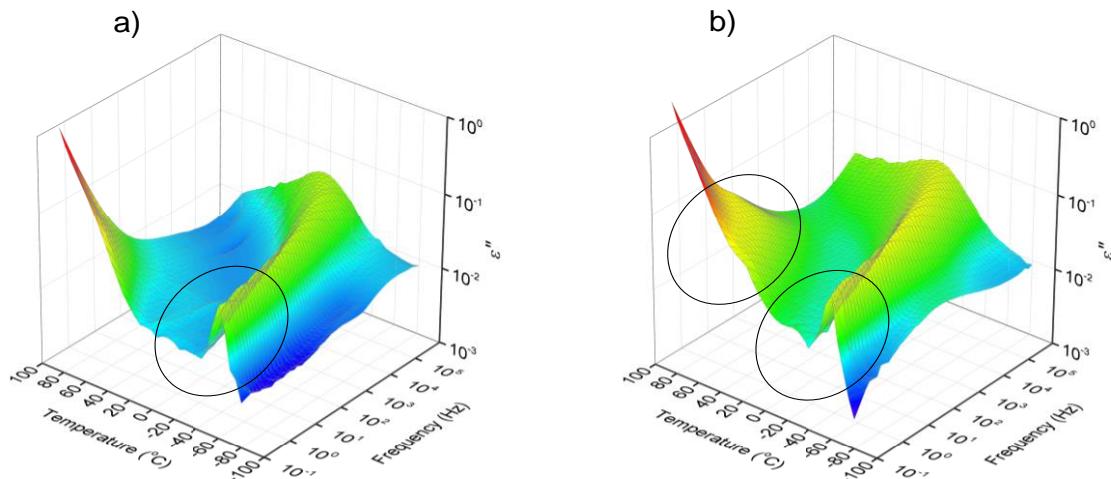


Figure 5. Representative 3-D plot of NR/0.5 graphene nanocomposites: a) pristine; b) healed at 70 °C. Marked zones correspond to the segmental (low temperature) and interfacial (high temperature) relaxation regions.

Starting with the segmental relaxation, all the pristine nanocomposites exhibit similar profiles, indicating that graphene content has little effect on the segmental dynamics (see Figure 6). Similar results were also reported by Tang *et al* in NR composites with graphene and graphene oxide (GO) contents up to 7 phr.[28]

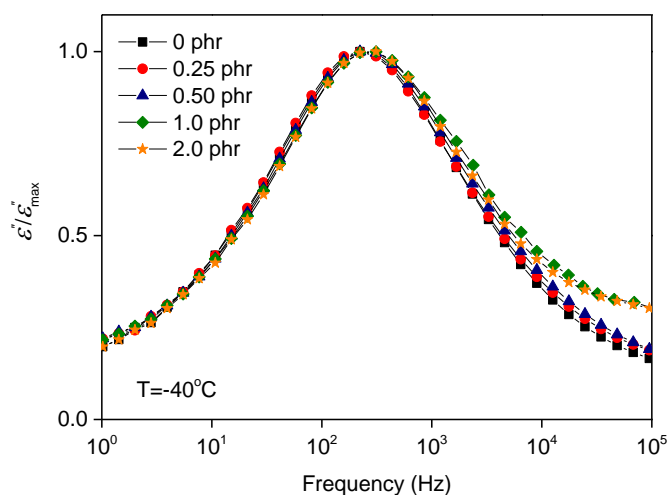


Figure 6. Normalized dielectric loss versus frequency of pristine NR/graphene nanocomposites as function of graphene content at $T = -40^\circ\text{C}$.

However, when damaged nanocomposites are thermally treated ($T = 70^\circ\text{C}$), a slight shift of the segmental relaxation process towards lower frequencies is revealed (see Figure 7) indicating that the relaxation times of the nanocomposites increase with healing. It seems that the thermal treatment (healing) leads to enhanced physicochemical interactions between the polymer matrix and the filler thereof slowing down the dynamics of the rubber segments. In fact, such an effect is not seen in the healed unfilled rubber (Figure 7a) where the only visible change with healing is on the network structure (appearance of a shoulder on the low frequency side), as previously reported.[16]

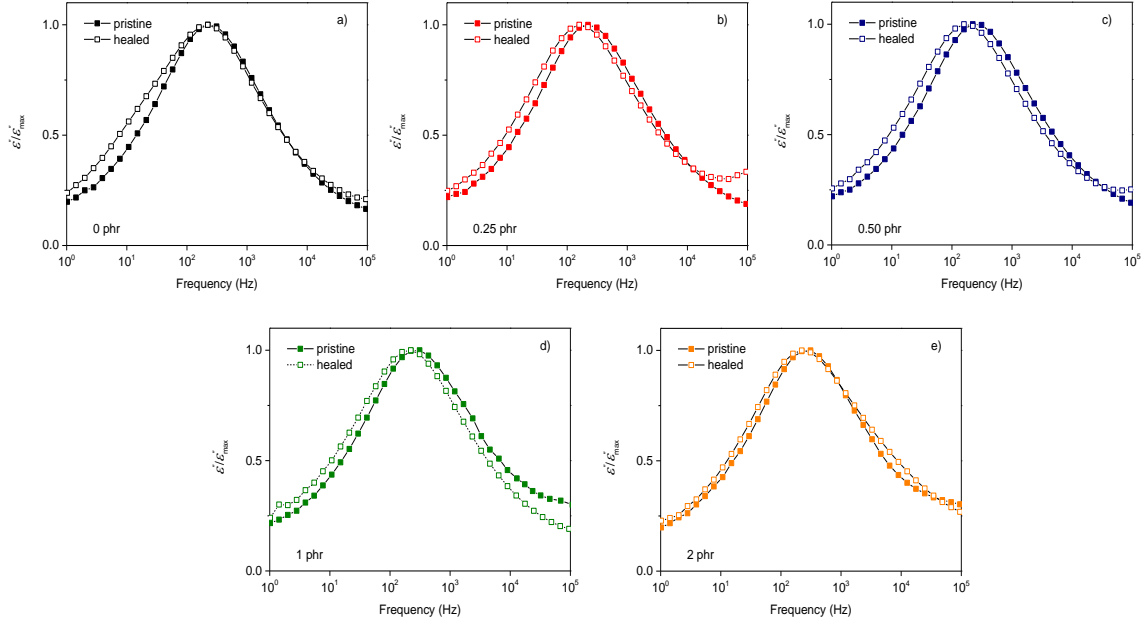


Figure 7. Normalized dielectric loss of NR/graphene nanocomposites as function of graphene content at $T=-40\text{ }^{\circ}\text{C}$: a) 0 phr; b) 0.25 phr; c) 0.50 phr; d) 1.0 phr; e) 2.0 phr. Solid and empty symbols represent pristine and healed (at $70\text{ }^{\circ}\text{C}$) samples, respectively.

The second relaxation to be discussed only appears in the healed nanocomposites (Figure 5b) and is suggested to be related to the restricted mobility of the polymer chains at the rubber-filler interface.[29,30] Figure 8a-c shows the dielectric loss vs frequency spectra of the healed NR/graphene nanocomposites with different graphene content at a representative temperature ($T=45\text{ }^{\circ}\text{C}$) in the region of the interfacial relaxation. All spectra have been deconvoluted using the Havriliak-Negami (HN) function.[30] The healed NR/0.25 graphene nanocomposite is omitted since the signal of the interfacial relaxation is too weak to be detected. Two trends can be extracted from these spectra: (i) an increase in the intensity of the interfacial relaxation and a shift of the maxima (f_{max}) to lower frequencies as graphene loading increases, and (ii) the absence of such relaxation in a pristine (non-damaged) sample subjected to the same healing thermal treatment and used as control sample (see Figure 8d). All facts suggest that higher mobility restrictions due to the presence of graphene come into play as a result of the thermal healing treatment. This new relaxation is attributed to the formation of a new interface, but more specifically to the enhanced rubber-filler interactions at the newly created interface that increase with graphene loading. As will be presented in the next section, this aspect will play a major role in the healing process.

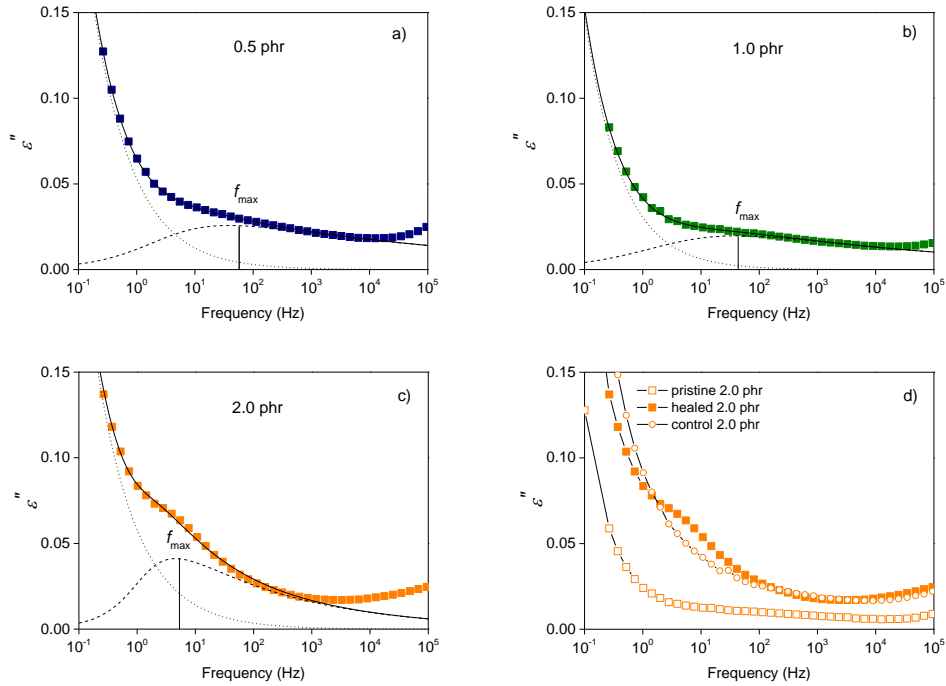


Figure 8. Interfacial relaxation at a selected temperature ($T=45\text{ }^{\circ}\text{C}$): a-c) healed NR/graphene nanocomposites with different graphene content. Solid lines represent the total fit, dashed lines the individual process and dotted lines the conductivity contribution; d) comparison between pristine, control and healed NR/2.0 phr graphene nanocomposites.

3.4. Restoration of mechanical, electrical and thermal properties as function of graphene content

Figure 9 presents the calculated healing efficiency values for the different functionalities as a function of the graphene loading. The underlying self-healing mechanism for pure vulcanized natural rubber is reported elsewhere.[16,17] Concerning the thermal conductivity, it decreases upon damage for all material grades (see Figure 4) as the rough surface of the damaged sample promotes air gaps between the sample and the aluminum foil. After healing, thermal conductivity can be completely restored indicating a good wetting of the materials on the aluminum foil (disappearance of air gaps) due to the enhanced flow capability of the nanocomposites during the high temperature healing step, irrespective of the amount of graphene included in the rubber nanocomposite (see η_{thermal} in Figure 9). With respect to electrical conduction, when micro- or macro- cracks are formed in the rubber nanocomposite the connection of fillers may break down. Since the electrical conductivity of composites depends on the connection of fillers, the damage leads to a decrease of electrical conductivity.[11] However, after healing such a connection seems to be re-established and

electrical conductivity restored (see Figure 3b). A significant upturn in electrical healing efficiency seems to be located above the electrical percolation threshold (see $\eta_{\text{electrical}}$).

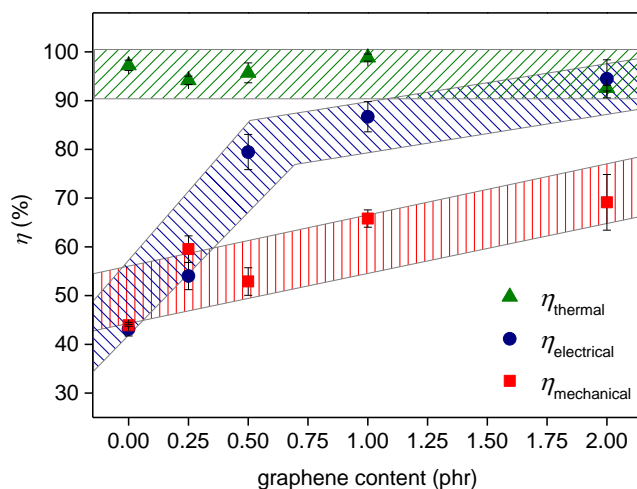


Figure 9. Overall healing of multi-functionalities of NR/graphene nanocomposites healed at $T=70\text{ }^{\circ}\text{C}$, as function of graphene content.

On the other hand, mechanical healing efficiency ($\eta_{\text{mechanical}}$) based on the recovery of tensile strength, tends to increase only gradually with graphene content reaching a maximum of $\sim 70\%$ with 2.0 phr graphene. As stated above, high graphene loadings result in a less crosslinked rubber network. This result is in agreement with our previous studies with self-healing rubbers and hard dual networks where faster healing kinetics were obtained for lower crosslinking densities.[17,31] From the results herein shown, it is therefore expected that higher graphene loading results in higher healing efficiency. A further explanation to these results can be the improvement of the interfacial adhesion with the thermal healing treatment.[12] When temperature is applied rubber chains can be physically adsorbed on adjacent graphene layers promoting the interaction between the diffused rubber chains and the graphene sheets at the interface.[15,32] Evidences of such enhanced interactions are the restricted segmental relaxation and the appearance of the interfacial relaxation at high temperatures, as previously discussed by FT-IR and BDS. Hence, these rubber-filler interactions plus the lower crosslinking density seem to be crucial parameters contributing to the higher healing efficiency at higher graphene loading.

We now like to discuss and compare the healing efficiencies for the three properties for the whole range of graphene content. The restoration of thermal properties seems to be more feasible (higher healing values) since the main requirement to be met for the recovery is a

good contact between the two broken parts (interface formation). Electrical healing, on the other hand, requires similar surface contact as for thermal healing plus intimate particle-to-particle contact assuring the creation of an electrical conducting path, with the graphene percolation threshold set as the lower limit for healing to occur. However, mechanical recovery needs to fulfill different settings based on the formation of a new interphase: *i*) good contact between damaged surfaces, *ii*) good particle-to-particle contact and good rubber-filler interactions at the interface, and *iii*) effective load transfer at the interface in order to achieve the full restoration of the original polymeric network at the macroscale damaged interface.[16,33] It is therefore expected that the recovery of the mechanical properties appears as more demanding than the restoration of electrical and thermal conducting properties. Figure 10 summarizes these trends schematically showing the minimal requirements to be met and how to link them to the healing of different functionalities.





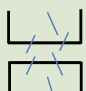

Functionality	Damaged sample	Healed sample	Minimal requirements for healing	Graphene content effect on healing
thermal			1-Surface contact	Independent
electrical			1-Surface contact 2- Percolation path	Percolation threshold set as lower limit
mechanical			1-Surface contact 2- Rubber-filler interactions 3- Load transfer at the interface	Gradual increase

Figure 10. Schematic representation showing the minimal requirements to be met for restoring thermal, electrical and mechanical functionalities.

4. Conclusions

Self-healing graphene/natural rubber nanocomposites were compounded and their mechanical, electrical and thermal properties evaluated before and after healing. The nanoscale morphology of the composites revealed good dispersion but low rubber-filler adhesion, reflecting modest mechanical enhancement and moderate electrical and thermal conduction. After damage and thermal treatment (healing) full or partial recovery of the functionalities was observed. Graphene content was found to have a different effect for each property: *i*) thermal conductivity healing was complete even at the lowest graphene content; *ii*) electrical conductivity healing was low at low contents but became high at the electrical

percolation limit; and *iii*) mechanical healing gradually increased with graphene content to a maximal level of 70%. The molecular dynamics analysis revealed the key role of rubber-graphene interactions at the healed interphase on the overall restoration of the different functionalities. The (indirect) dependence of healing efficiency of the three functionalities on graphene content is probably due to a combination of the lower crosslinking density due to the graphene presence, as well as the formation of strong rubber-graphene interactions at the healed interphase.

Acknowledgements

M. Hernández thanks the European Commission for a Marie Curie Fellowship (PIEF-GA-2013-623379).

References

- [1] Potts J. R., Dreyer D. R., Bielawski C. W., Ruoff R. S. Graphene-based polymer nanocomposites. *Polymer*. 2011;52(1):5-25.
<http://dx.doi.org/10.1016/j.polymer.2010.11.042>
- [2] Sadasivuni K. K., Ponnamma D., Thomas S., Grohens Y. Evolution from graphite to graphene elastomer composites. *Progress in Polymer Science*. 2014;39(4):749-780.
<http://dx.doi.org/10.1016/j.progpolymsci.2013.08.003>
- [3] Potts J. R., Shankar O., Murali S., Du L., Ruoff R. S. Latex and two-roll mill processing of thermally-exfoliated graphite oxide/natural rubber nanocomposites. *Composites Science and Technology*. 2013;74:166-172.
<http://dx.doi.org/10.1016/j.compscitech.2012.11.008>
- [4] Potts J. R., Shankar O., Du L., Ruoff R. S. Processing-Morphology-Property Relationships and Composite Theory Analysis of Reduced Graphene Oxide/Natural Rubber Nanocomposites. *Macromolecules*. 2012;45(15):6045-6055.
<http://dx.doi.org/10.1021/ma300706k>
- [5] Yaragalla S., Meera A. P., Kalarikkal N., Thomas S. Chemistry associated with natural rubber-graphene nanocomposites and its effect on physical and structural properties. *Industrial Crops and Products*. 2015;74:792-802.
<http://dx.doi.org/10.1016/j.indcrop.2015.05.079>
- [6] Zhan Y., Wu J., Xia H., Yan N., Fei G., Yuan G. Dispersion and Exfoliation of Graphene in Rubber by an Ultrasonically-Assisted Latex Mixing and In situ Reduction Process. *Macromolecular Materials and Engineering*. 2011;296(7):590-602.

<http://dx.doi.org/10.1002/mame.201000358>

[7] Luo Y. Y., Zhao P. F., Yang Q., He D. N., Kong L. X., Peng Z. Fabrication of conductive elastic nanocomposites via framing intact interconnected graphene networks. *Composites Science and Technology*. 2014;100:143-151.

<http://dx.doi.org/10.1016/j.compscitech.2014.05.037>

[8] Wu J., Xing W., Huang G., Li H., Tang M., Wu S., Liu Y. Vulcanization kinetics of graphene/natural rubber nanocomposites. *Polymer*. 2013;54(13):3314-3323.

<http://dx.doi.org/http://dx.doi.org/10.1016/j.polymer.2013.04.044>

[9] Hernandez M., Bernal M. D., Verdejo R., Ezquerro T. A., Lopez-Manchado M. A. Overall performance of natural rubber/graphene nanocomposites. *Composites Science and Technology*. 2012;73:40-46.

<http://dx.doi.org/10.1016/j.compscitech.2012.08.012>

[10] van der Zwaag S., Grande A. M., Post W., Garcia S. J., Bor T. C. Review of current strategies to induce self-healing behaviour in fibre reinforced polymer based composites. *Materials Science and Technology*. 2014;30(13A):1633-1641.

<http://dx.doi.org/10.1179/1743284714y.0000000624>

[11] Zhong N., Post W. Self-repair of structural and functional composites with intrinsically self-healing polymer matrices: A review. *Composites Part A Applied Science and Manufacturing*. 2015;69:226-239.

<http://dx.doi.org/10.1016/j.compositesa.2014.11.028>

[12] Xiao X. C., Xie T., Cheng Y. T. Self-healable graphene polymer composites. *Journal of Materials Chemistry*. 2010;20(17):3508-3514.

<http://dx.doi.org/10.1039/c0jm00307g>

[13] Wang C., Liu N., Allen R., Tok J. B. H., Wu Y. P., Zhang F., Chen Y. S., Bao Z. N. A Rapid and Efficient Self-Healing Thermo-Reversible Elastomer Crosslinked with Graphene Oxide. *Advanced Materials*. 2013;25(40):5785-5790.

<http://dx.doi.org/10.1002/adma.201302962>

[14] Huang L., Yi N., Wu Y., Zhang Y., Zhang Q., Huang Y., Ma Y., Chen Y. Multichannel and Repeatable Self-Healing of Mechanical Enhanced Graphene-Thermoplastic Polyurethane Composites. *Advanced Materials*. 2013;25(15):2224-2228.

<http://dx.doi.org/10.1002/adma.201204768>

[15] Liu J. Q., Song G. S., He C. C., Wang H. L. Self-Healing in Tough Graphene Oxide Composite Hydrogels. *Macromolecular Rapid Communications*. 2013;34(12):1002-1007.

<http://dx.doi.org/10.1002/marc.201300242>

[16] Hernández M., Grande A. M., van der Zwaag S., García S. J. Monitoring Network and Interfacial Healing Processes by Broadband Dielectric Spectroscopy: A Case Study on Natural Rubber. *ACS Applied Materials & Interfaces*. 2016;8(16):10647-10656.

<http://dx.doi.org/10.1021/acsami.6b02259>

[17] Hernández M., Grande A. M., Dierkes W., Bijleveld J., van der Zwaag S., García S. J. Turning Vulcanized Natural Rubber into a Self-Healing Polymer: Effect of the Disulfide/Polysulfide Ratio. *ACS Sustainable Chemistry & Engineering*. 2016;4(10):5776-5784.

<http://dx.doi.org/10.1021/acssuschemeng.6b01760>

[18] Bailey B. M., Leterrier Y., Garcia S. J., van der Zwaag S., Michaud V. Electrically conductive self-healing polymer composite coatings. *Progress in Organic Coatings*. 2015;85:189-198.

<http://dx.doi.org/10.1016/j.porgcoat.2015.04.013>

[19] Zhong N., Garcia S. J., Van Der Zwaag S. The effect of filler parameters on the healing of thermal conductivity and mechanical properties of a thermal interface material based on a self-healable organic-inorganic polymer matrix. *Smart Materials and Structures*. 2016;25(8).

<http://dx.doi.org/10.1088/0964-1726/25/8/084016>

[20] Flory P. J., Rehner J. Statistical mechanics of cross-linked polymer networks II Swelling. *Journal of Chemical Physics*. 1943;11(11):521-526.

<http://dx.doi.org/10.1063/1.1723792>

[21] Lorenz O., Parks C. R. The crosslinking efficiency of some vulcanizing agents in natural rubber. *Journal of Polymer Science*. 1961;50(154):299-312.

<http://dx.doi.org/10.1002/pol.1961.1205015404>

[22] Zhong B. C., Jia Z. X., Hu D. C., Luo Y. F., Guo B. C., Jia D. M. Surface modification of halloysite nanotubes by vulcanization accelerator and properties of styrene-butadiene rubber nanocomposites with modified halloysite nanotubes. *Applied Surface Science*. 2016;366:193-201.

<http://dx.doi.org/10.1016/j.apsusc.2016.01.084>

[23] Haseena A. P., Dasan K. P., Namitha R., Unnikrishnan G., Thomas S. Investigation on interfacial adhesion of short sisal/coir hybrid fibre reinforced natural rubber composites by restricted equilibrium swelling technique. *Composite Interfaces*. 2004;11(7):489-513.

<http://dx.doi.org/10.1163/1568554042722955>

[24] Toki S., Burger C., Hsiao B. S., Amnuayporn Sri S., Sakdapipanich J., Tanaka Y. Multi-Scaled Microstructures in Natural Rubber Characterized by Synchrotron X-Ray Scattering

and Optical Microscopy. *Journal of Polymer Science Part B: Polymer Physics*. 2008;46(22):2456-2464.

<http://dx.doi.org/10.1002/polb.21578>

[25] Tiwari S. K., Choudhary R. N. P., Mahapatra S. P. Effect of multiwalled carbon nanotube and temperature on dielectric and impedance spectroscopy of chlorobutyl elastomer nanocomposites. *Journal of Elastomers and Plastics*. 2015;47(6):549-572.

<http://dx.doi.org/10.1177/0095244314526742>

[26] Bokobza L. Multiwall carbon nanotube elastomeric composites: A review. *Polymer*. 2007;48(17):4907-4920.

<http://dx.doi.org/10.1016/j.polymer.2007.06.046>

[27] Moniruzzaman M., Winey K. I. Polymer nanocomposites containing carbon nanotubes. *Macromolecules*. 2006;39(16):5194-5205.

<http://dx.doi.org/10.1021/ma060733p>

[28] Tang Z. H., Zhang L. Q., Feng W. J., Guo B. C., Liu F., Jia D. M. Rational Design of Graphene Surface Chemistry for High-Performance Rubber/Graphene Composites. *Macromolecules*. 2014;47(24):8663-8673.

<http://dx.doi.org/10.1021/maS02201e>

[29] Vo L. T., Anastasiadis S. H., Giannelis E. P. Dielectric study of Poly(styrene-co-butadiene) Composites with Carbon Black, Silica, and Nanoclay. *Macromolecules*. 2011;44(15):6162-6171.

<http://dx.doi.org/10.1021/ma200044c>

[30] Hernández M., Carretero-Gonzalez J., Verdejo R., Ezquerro T. A., López-Manchado M. A. Molecular dynamics of natural rubber/layered silicate nanocomposites as studied by dielectric relaxation spectroscopy. *Macromolecules*. 2010;43(2):643-651.

<http://dx.doi.org/10.1021/ma902379t>

[31] Abdolah Zadeh M., Grande A. M., van der Zwaag S., Garcia S. J. Effect of curing on the mechanical and healing behaviour of a hybrid dual network: a time resolved evaluation. *RSC Advances*. 2016;6(94):91806-91814.

<http://dx.doi.org/10.1039/C6RA17799A>

[32] Ramanathan T., Abdala A. A., Stankovich S., Dikin D. A., Herrera-Alonso M., Piner R. D., Adamson D. H., Schniepp H. C., Chen X., Ruoff R. S., Nguyen S. T., Aksay I. A., Prud'homme R. K., Brinson L. C. Functionalized graphene sheets for polymer nanocomposites. *Nature Nanotechnology*. 2008;3(6):327-331.

<http://dx.doi.org/10.1038/nnano.2008.96>

[33] Grande A. M., Bijleveld J. C., Garcia S. J., van der Zwaag S. A combined fracture mechanical - rheological study to separate the contributions of hydrogen bonds and disulphide linkages to the healing of poly(urea-urethane) networks. *Polymer*. 2016;96:26-34.

<http://dx.doi.org/10.1016/j.polymer.2016.05.004>

List of Figures

Figure 1. FT-IR spectra of NR/graphene nanocomposites: a) whole wavenumber range; b) at selected normalized region. Solid lines and dashed lines correspond to pristine and healed samples, respectively.

Figure 2. SEM images of pristine NR/graphene nanocomposites with different graphene loading: a) 0.25 phr; b) 0.5 phr; c) 1.0 phr; d) 2.0 phr; e) 2.0 phr at higher magnification.

Figure 3. a) Electrical conductivity of pristine NR/graphene nanocomposites as function of frequency with graphene content as a parameter; b) Electrical conductivity of NR/graphene nanocomposites pristine and healed (at 70 °C), at a frequency of $f=10^{-1}$ Hz.

Figure 4. Relative thermal conductivity of pristine, damaged and healed NR/graphene nanocomposites as function of graphene content measured at room temperature.

Figure 5. Representative 3-D plot of NR/0.5 graphene nanocomposites: a) pristine; b) healed at 70 °C. Marked zones correspond to the segmental (low temperature) and interfacial (high temperature) relaxation regions.

Figure 6. Normalized dielectric loss versus frequency of pristine NR/graphene nanocomposites as function of graphene content at $T=-40$ °C.

Figure 7. Normalized dielectric loss of NR/graphene nanocomposites as function of graphene content at $T=-40$ °C: a) 0 phr; b) 0.25 phr; c) 0.50 phr; d) 1.0 phr; e) 2.0 phr. Solid and empty symbols represent pristine and healed (at 70 °C) samples, respectively.

Figure 8. Interfacial relaxation at a selected temperature ($T=45$ °C): a-c) healed NR/graphene nanocomposites with different graphene content. Solid lines represent the total fit, dashed lines the individual process and dotted lines the conductivity contribution; d) comparison between pristine, control and healed NR/2.0 phr graphene nanocomposites.

Figure 9. Overall healing of multi-functionalities of NR/graphene nanocomposites healed at $T=70$ °C, as function of graphene content.

Figure 10. Schematic representation showing the minimal requirements to be met for restoring thermal, electrical and mechanical functionalities.

List of Tables

Table 1. NR compound recipe.

Table 2. Swelling ratio and crosslinking density of pristine NR/graphene nanocomposites.

Table 3. Tensile properties of pristine and healed NR/graphene nanocomposites.